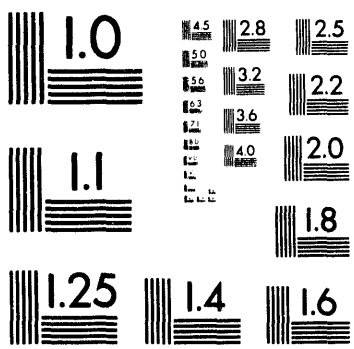
1.0
1.1
1.25
1.4
1.6
1.8
2.0
2.2
2.5
2.8
3.2
3.6
4.0
4.5
5.0
5.6
6.3
7.1

1 of 1

DOE/ER/13519-7

EXPERIMENTAL STUDY OF INTERACTIONS OF HIGHLY CHARGED IONS WITH ATOMS AT keV ENERGIES

~~Final~~ Progress Report

for the Period

August 15, 1990 - February 15, 1993

V.O. Kostroun

Cornell University
Ithaca, New York 14853

January 29, 1993

Prepared for
THE U.S. DEPARTMENT OF ENERGY
GRANT NO. DE-FG02-86ER13519

Abstract

This final progress report summarizes the work carried out during the 29 month period from August 15, 1990 to February 15, 1993 under grant DE-FG02-86ER13519.

The following experiments were done. We measured the absolute total and one- and two- electron transfer cross sections for Ar^{q+} ($8 \leq q \leq 16$) on He and H_2 at 2.3 qkeV, the angular distributions of the scattered projectiles in $Ar^{8+,9+}$ collisions with Ar and Kr at 2.3 qkeV, the electron emissions in low energy Ar^{q+} on Ar collisions, the recoil ion charge state distributions in low energy Ar^{q+}-Ar collisions, the absolute total and one-and two-electron transfer cross sections for Ar^{8+} on Ar at 2.3 qkeV, and the absolute total and one- and two-electron transfer cross sections for Ar^{8+} on Ar as a function of energy. We also used energy gain spectroscopy to study Ar^{q+} on Ar collisions at 40 and 30 qeV, and time of flight spectroscopy to investigate ionization and dissociation of CO and N_2 in collisions with low energy, highly charged argon ions.

In addition, we applied the Goldberger and Watson transition theory to derive transition rates and cross sections for atomic radiative and/or non radiative processes, wrote a computer code TRANSIT which can calculate energies, wave functions and radiative and non radiative rates for atoms and ions. The code is highly modular and can easily be modified to calculate higher order processes. Finally, we have done an Ab-Initio molecular orbital electronic energy level calculation for the $(ArAr)^{8+}$ system as a function of internuclear separation.

Some of the experiments have been published in final form, others in preliminary versions, and some remain to be analyzed.

Table of contents

Introduction

Experimental study of low energy, highly charged ions with other atomic species requires an advanced ion source such as an electron beam ion source, EBIS [1] or an electron cyclotron ion source, ECRIS [2]. Over the past few years, a significant portion of our effort has gone into the design and construction of an electron beam ion source capable of producing the ions of interest.

The essential components of an EBIS are a magnetic solenoid, an electron gun, trapping electrode structure and an electron collector-ion extractor. The gun forms a beam which is focused and compressed by the magnetic field to a current density of ~1000 A/cm^2. The trapping electrode structure, concentric with the electron beam, and the beam space charge potential form an electrostatic trap in the axial and radial directions respectively. The ions trapped in the high current density electron beam are either ionized or excited, and at the end of a predetermined confinement time, the potential distribution applied to the trapping structure is changed to expel the ions from the trap. At the collector-extractor, the electron beam is collected and the ions extracted from the source. The kinetic energy of the extracted ions is determined by the potential applied to the trap electrodes and typically is of the order of a few keV/charge.

A few months before the start of the current grant period, we finished construction of the Cornell superconducting solenoid, cryogenic EBIS (CEBIS), figure 1.

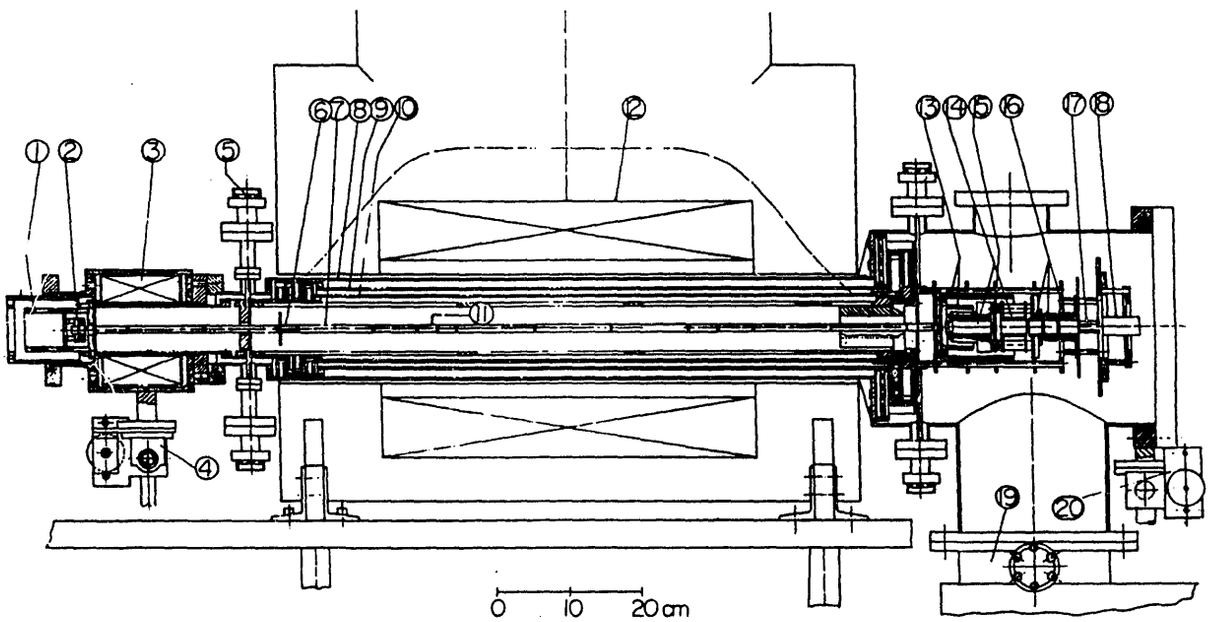

Figure 1. Schematic diagram of the Cornell superconducting solenoid, cryogenic EBIS. 1) electron gun magnetic shield, 2) electron gun, 3) entrance solenoid, 4) gun-end vacuum chamber linear positioner, 5) gun-end drift-tube positioners, 7) drift tube, 8) main vacuum chamber, 9) 77 ^{o}K

thermal shield, 10) 30 ^{o}K copper cryopanel, 11) gas inlet, 12) 3 Tesla main solenoid, 13)electron-collector magnetic shield, 14) electron collector, 15) ion extractor, 16) einzel lens, 17) time-of-flight chopper plates, 18) horizontal deflection plates, 19) cryopump, 20) collector-end vacuum-chamber linear positioner.

CEBIS is designed around a warm bore, 6.0" diameter, 31" long, 3 Tesla superconducting solenoid. The solenoid was made by Nicolet Instruments Corp., Madison, WI, and is identical to solenoids used in the Nicolet Fourier transform mass spectrometry system. (Now manufactured by EXTREL FTMS, Madison, WI.) The warm bore and inexactly known location of the solenoid magnetic axis required a design different from those based on the Dubna, Russia KRION [3] and Orsay/Saclay, France CRYEBIS [4] sources. The CEBIS vacuum chamber which houses the EBIS structure can be moved and aligned with the magnetic axis of the solenoid. In addition to the adjustable vacuum chamber, the EBIS drift tube structure itself can be positioned independently with respect to the vacuum chamber. The drift tube structure, together with the electron collector-ion extractor and some ion optics can all be removed from the source as one unit. Ultra high vacuum in the interaction region is provided by a large surface copper panel cryopump cooled to 30 ^{o}K. CEBIS uses a system of external gun injection that does not require a magnetic field buildup tailored to a specific electron gun. The electron beam is injected into and focused by a short conventional solenoid. Once the beam is established, it is adiabatically compressed by the fringe field of the main solenoid.

CEBIS uses a commercial electron gun, Litton Model M-707, which is rated for 10 kV and has a perveance of 0.25 microperv. Thus far we have operated the gun below 2.5 kV. With 2.5 kV on the cathode and 2-4.5 kV on the drift tubes, we have a 4.5-7.0 keV, 30 mA electron beam, transmitted through the source with 99% transmission efficiency. For the time being, we operate the gun at lower cathode potentials to minimize damage to the internal drift tube structure should the beam wander for some reason.

The various degrees of freedom of the vacuum chamber and drift tube structure with respect to the magnetic axis of the solenoid have allowed us to explore the behavior of the source when misaligned. We have found that the most critical misalignments are connected with the electron gun and collector. In particular, misalignment of the electron beam with the magnetic field lines entering and exiting the main solenoid, or, what is worse, the attachment of the beam to field lines at the entrance solenoid that then do not end up on the collector, contribute more than anything else to poor source performance. Such misalignments appear to have a much greater effect on source performance than straightness of the magnetic field, alignment of the drift tube structure with the electron beam or the quality of vacuum in the source. Good operation of the ion source in a restricted range of operating parameters is symptomatic of misalignments of the electron beam with the magnetic field at the entrance into, and exit out of the main solenoid region. In these cases,

one may find for example, that as the cathode voltage is increased, electron beam transmission through the source decreases with increasing electron current. Most EBIS sources in existence exhibit such behavior to some extent.

CEBIS is competitive with existing EBIS sources in terms of ion output and the ion charge state distribution produced, figure 2. Because the magnet operates in the persistent current mode and is very well shielded thermally, the source has very low cryogen consumption (50 liters

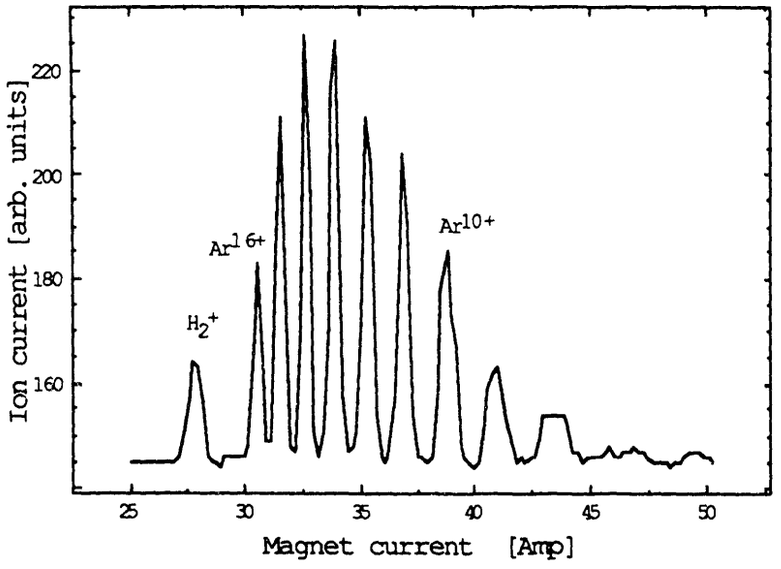

Figure 2. Ion output from CEBIS The ions were produced by a 17 mA, 3.5 keV (-1.5 kV on the cathode and 2.0 kV on the drift tubes) electron beam. The confinement time was 90 ms.

LHe and 200 liters LN_2 per month respectively). The source can be turned on in the morning, off in the evening and can run virtually unattended for weeks at a time. CEBIS is a compact and economical device, easy to operate, maintain and repair. The source can be warmed up, opened, repaired, modified, etc. closed up and cooled down in three days. It operates reliably and is not restricted to a small range of operating parameters. The Nicolet solenoid is unshielded, but the magnetic field at the beam line and experimental chambers has not created any great difficulties.

In addition to the ion source, we have constructed a beam transport system, several experimental vacuum chambers, gas targets, an atomic hydrogen microwave discharge source, and different electrostatic analyzers. We have built a versatile collision chamber from a discarded plasma experiment stainless steel vacuum chamber that is 24" in diameter and 24" long. The chamber is pumped on by a 170 l/s Balzers turbomolecular pump, a 2400 l/s (air) Varian VHS-6 and a 1200 l/s (air) VHS-4 diffusion pump. The base pressure with apparatus in place is 3×10^{-8} Torr. The collision chamber contains ion decelerating optics, four 180^{o} spherical electrostatic

analyzers, and a gas target. It is versatile in that all electrical connections are made inside the chamber to a "distribution panel", and connections from the "panel" to feedthroughs are not disturbed. In effect, the experiments are built on a small "table top" mounted inside the chamber and it is very easy to change from one experiment to another in a matter of hours. An atomic target microwave discharge source and a 2m long time-of-flight spectrometer can be attached to ports on the collision chamber.

Two of the 180^{o} spherical analyzers are connected in tandem to monochromatize the beam and the other two, also connected in tandem are used to analyze the beam after it has passed through the interaction region. The experimental arrangement is similar to that commonly used in translational spectroscopy experiments. [5] The 180^{o} spherical analyzers have a 3.5" mean radius and the separation between the spherical surfaces is 0.4". For a 2 mm wide beam from the source, the $\Delta E/E$ is 0.011. The analyzers are machined from aluminum, which was copper and then gold plated.

Experimental work finished

Over the past two and a quarter years, the ion source and the experimental apparatus have been used continuously to carry out a number of experiments involving low energy, highly charged ions. In this section we describe the experiments that were finished and their present status. Some of the experiments are described in greater detail in reprints of papers in the appendix.

1) Absolute total and one and two electron transfer cross sections for Ar^{q+} $(8 \le q \le 16)$ on He and H_2 at 2.3 qkeV

The absolute values for the total, one and two electron transfer cross sections were measured by the growth rate method. [6] Selected Ar charge states passed through a gas cell, after which they were charge state analyzed by a $\pi\sqrt{2}$ cylindrical electrostatic analyzer and the ions detected by a channeltron operated in the current mode, figure 3. The pressure in the gas cell, figure 4, can be measured absolutely by the orifice flow method used for absolute pressure gauge calibration. [7,8] The gas cell is of our design, and consists of two cylindrical chambers, the lower one being the target. The conductances of the ion beam entrance and exit apertures are calculated and added to give a total conductance C_2. Target gas is admitted into the upper chamber, and flows into the target cell through a very small conductance C_1 which is measured. The pressure P_c in the gas cell is given by

$$P_c = \frac{C_1 P_1}{C_1 + C_2}$$

where P_1, the pressure in the upper chamber, is measured by a capacitance manometer. The experimental cross sections obtained are shown in figures 5 and 6. The overall error in the Ar^{q+} on H_2 cross section measurement is ±10%, and for He, ±15%.

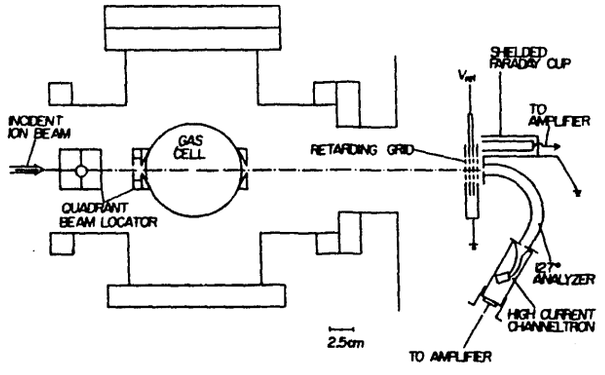

Figure 3 Experimental arrangement used in the measurement of absolute cross sections.

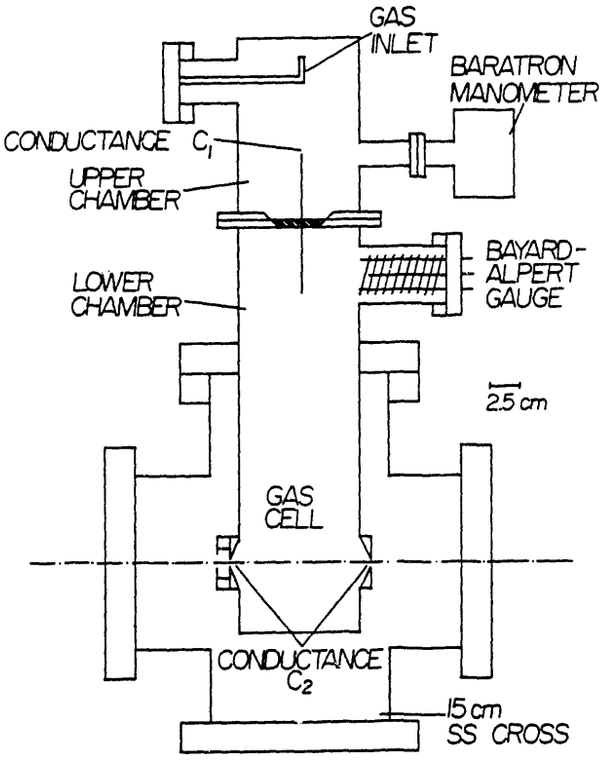

Figure 4. Schematic of gas target cell. For pressures in the vacuum chamber much smaller than P_c, the pressure in the lower chamber is given by $P_c = \frac{C_1 P_1}{C_1+C_2}$ where P_1 is the pressure in the upper chamber.

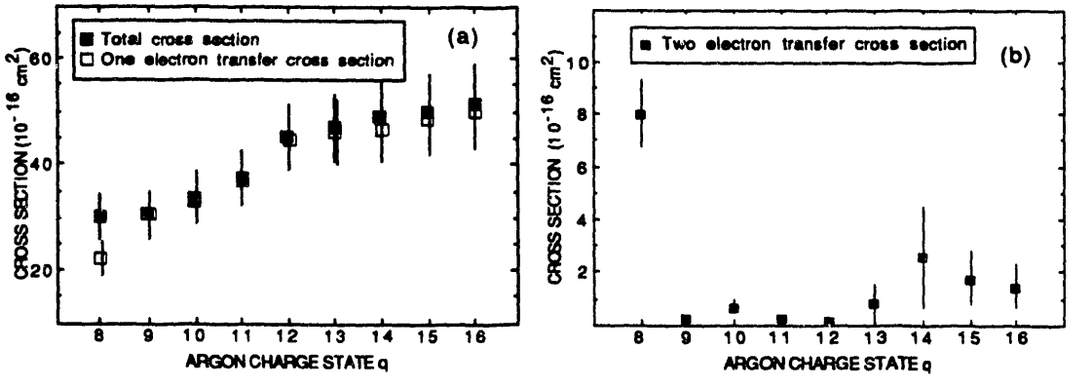

Figure 5 (a) Total and one electron transfer cross sections for Ar^q on He at 2.3 qkeV as a function of Ar charge state. (b) Two electron transfer cross sections.

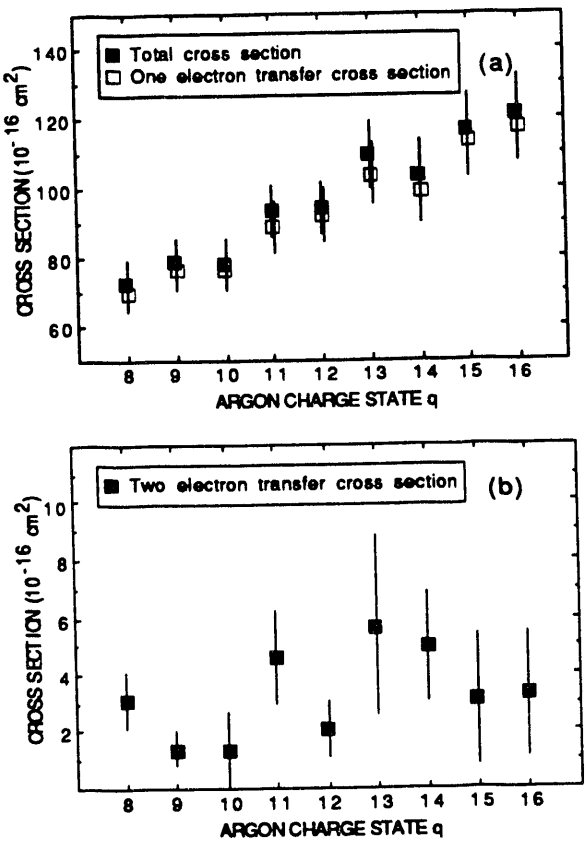

Figure 6 (a) Total and one electron transfer cross sections for Ar^q on H_2 at 2.3 qkeV as a function of Ar charge state. (b) Two electron transfer cross sections.

An article based on this work has been accepted for publication by Phys. Rev. A, and a preprint of this paper can be found in the appendix.

2) Angular distribution of the scattered projectiles in $Ar^{8+,9+}$ collisions with Ar and Kr at 2.3 qkeV

In this experiment, we measured the angular distribution of scattered projectiles in an attempt to learn more about collisions between low energy, highly charged ions and multielectron targets. Charge selected Ar^{8+} or Ar^{9+} ions entered a 25 mm long gas cell located 450 mm downstream from the focal point of our 90° analyzing magnet. The gas cell entrance and exit slits were 0.2 mm wide, 1.0 mm high, and 2 mm wide, 4 mm high respectively. A fixed horizontal slit, 0.65 mm wide, whose height could be adjusted, was located 890 mm from the gas cell entrance slit. A $\pi\sqrt{2}$ cylindrical electrostatic analyzer (mean radius 50 mm), mounted on a stage that could be moved perpendicular to the incident beam direction, was used to charge state analyze and scan the scattered beam. Ions were detected by a channeltron located behind the analyzer exit slit and operated in the current mode . The analyzer entrance slit, 0.4 mm wide, was 1140 mm from the

gas cell entrance slit. The data obtained for Ar^{9+} on Ar are shown in figures 7 and 8 which show both the direct (primary charge state, no gas) and scattered (charge decreased by one and two) beams. The raw data angle-energy product, θT, for one electron transfer is 0.81 x 20.7 or 16.6 mrad-keV. Assuming θT to be constant [9], one would expect at 1.35 keV θ to be 12.3 mrad. A recent angular distribution measurement using our new apparatus gave θ = 15.7 mrad at 1.35 keV In the latter experiment, the FWHM of the incident beam was about 8 mrad.

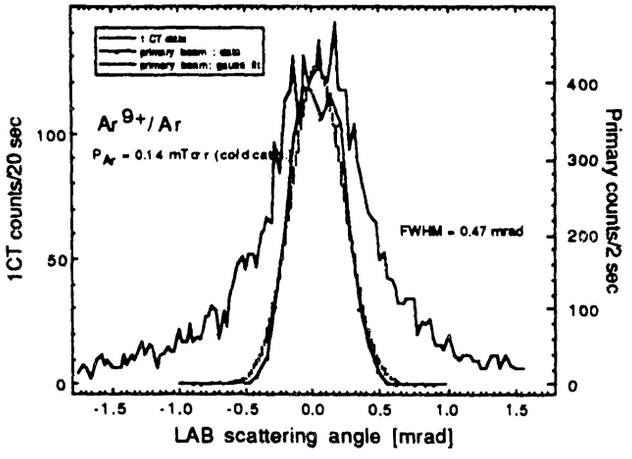

Figure 7. Angular distribution of the scattered projectiles in Ar^{9+} + Ar→Ar^{8+} at 2.3 qkeV laboratory energy. The distribution was recorded by stepping a $\pi\sqrt{2}$ electrostatic analyzer with a 0.4 mm wide entrance slit perpendicular to the incident beam direction. The analyzer was located 1140 mm from the short gas cell and set to pass Ar^{8+}.

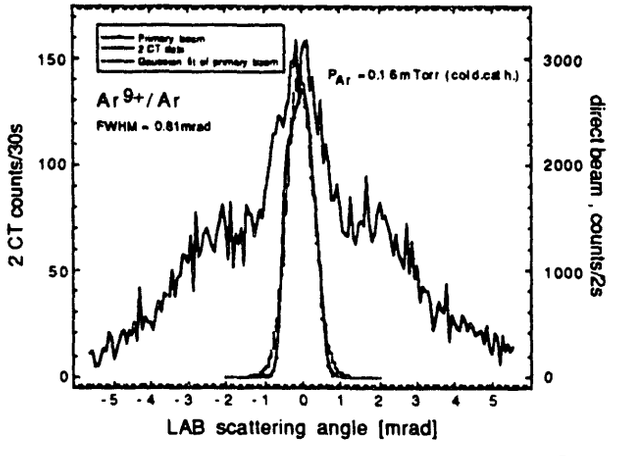

Figure 8. Angular distribution of the scattered projectiles in Ar^{9+} + Ar→Ar^{7+} at 2.3 qkeV laboratory energy. The distribution was recorded by stepping a $\pi\sqrt{2}$ electrostatic analyzer with a 0.4 mm wide entrance slit perpendicular to the incident beam direction. The analyzer was located 1140 mm from the short gas cell and set to pass Ar^{7+}.

This data remains to be analyzed.

3) Electron emissions in low energy Ar^{q+} on Ar collisions

It has been known for some time that in collisions of low energy, highly charged argon ions with argon, most projectiles undergo collisions in which the initial charge state decreases by one unit only. At the same time, the recoil target-ion charge state distribution contains ions whose charge state ranges form one to eight. Since singly charged recoil ions account for only one half of these ions, half of all collisions is accompanied by electron emission. By looking at the number and energy distribution of the emitted electrons, we expect to learn something about collisions between low energy, highly charged ions and multielectron targets.

Ar^{q+} $(8 \leq q \leq 16)$ ions were produced by the Cornell ion source CEBIS and extracted at 2.3 kV. Magnetically selected charge states passed through a gas cell containing argon at 7.5×10^{-4} Torr. Electrons emitted in the 30-400 eV energy range were analyzed at 90^{o} to the incident beam by a $\pi\sqrt{2}$ cylindrical electrostatic analyzer (mean radius 50 mm) figure 9. The source size, entrance slit width and dimensions of the analyzer were such that $\Delta E/E = 0.028$. All spectra were normalized to the same beam intensity. We chose to look at 90^{o} to maximize the source viewing angle. At 90^{o} the Doppler shift exhibits the greatest variation with angle, but at the low velocities in this experiment, 0.2 a.u. maximum, the estimated shift due to the spectrometer acceptance angle is only ± 1.5 eV at 400 eV electron energy. The electron spectra emitted in Ar^{14+} on Ar at 2.3 qkeV are shown in figure 10

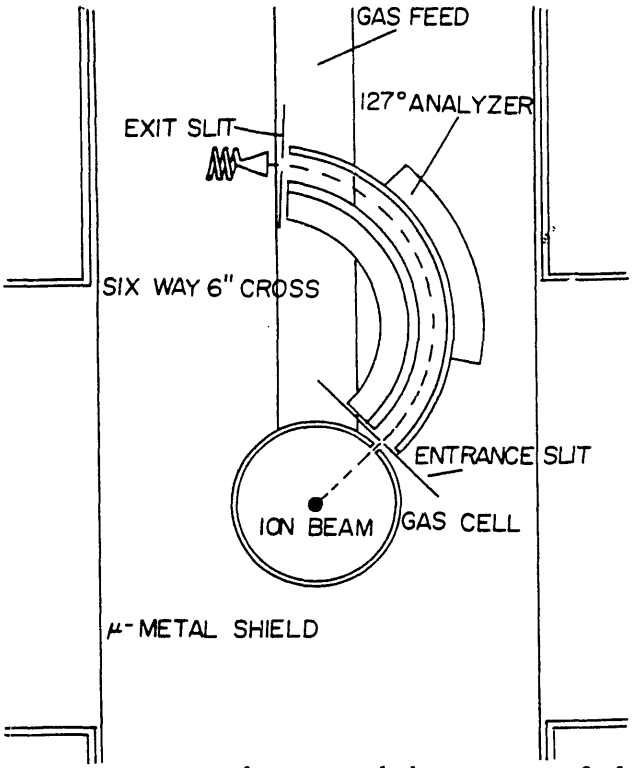

Figure 9. Experimental arrangement used to record the spectra of electrons emitted in Ar^{q+} $(8 \leq q \leq 18)$ collisions at 2.3 qkeV. View upstream.

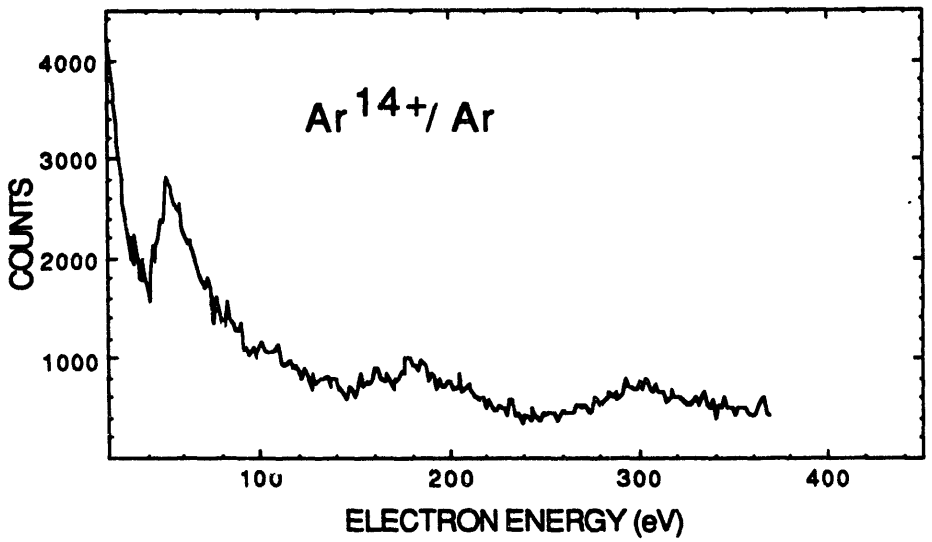

Figure 10. Spectrum of electrons emitted in the 60-400 eV range in Ar^{14+} on Ar collisions at 2.3 qkeV.

The spectra measured in this series are the first such ever recorded using an electron beam ion source as a source of low energy, highly charged ions. It was possible to record the spectra for the higher charge states over a period of 5-7 hours because of the very high stability and excellent emittance of our EBIS. Due to the latter, most of the extracted charge state could be focused downstream of the 90^{o} analyzing magnet at the gas target (located 3.0 m downstream from the EBIS source extractor) into a line source 1.0 mm in diameter!

This work was accepted for publication as a contributed paper in the proceedings of the VIth International Conference on the Physics of Highly Charged Ions held at Kansas State University, September 28-October 2, 1992. A preprint of this article can be found in the appendix.

The entire set of data is being analyzed and a more detailed paper based on this work is in preparation.

4) Recoil ion charge state distributions in low energy Ar^{q+}-Ar collisions

In low energy, highly charged ion-multielectron atom collisions, the target atoms often have many electrons removed and themselves become fairly ionized. [10] The appearance of several free electrons in the collision has been attributed to processes not always specified explicitly, but collectively referred to as transfer ionization. [11] In order to interpret our data on electron emissions, we measured the recoil ion charge state distribution in Ar^{q+} on Ar $(8 \leq q \leq 16)$ collisions at 2.3 and 0.18 qkeV by time of flight (TOF) spectroscopy.

Magnetically selected charge states were crossed with a gas jet located between the first two plates of a 2.5 m long TOF spectrometer, [12] figure 11. The incident ion beam was chopped by a several hundred nanosecond wide pulse and the recoil ions produced in the Ar^{q+} on Ar collision swept out of the interaction region by a few volts/cm electric field and analyzed by TOF.

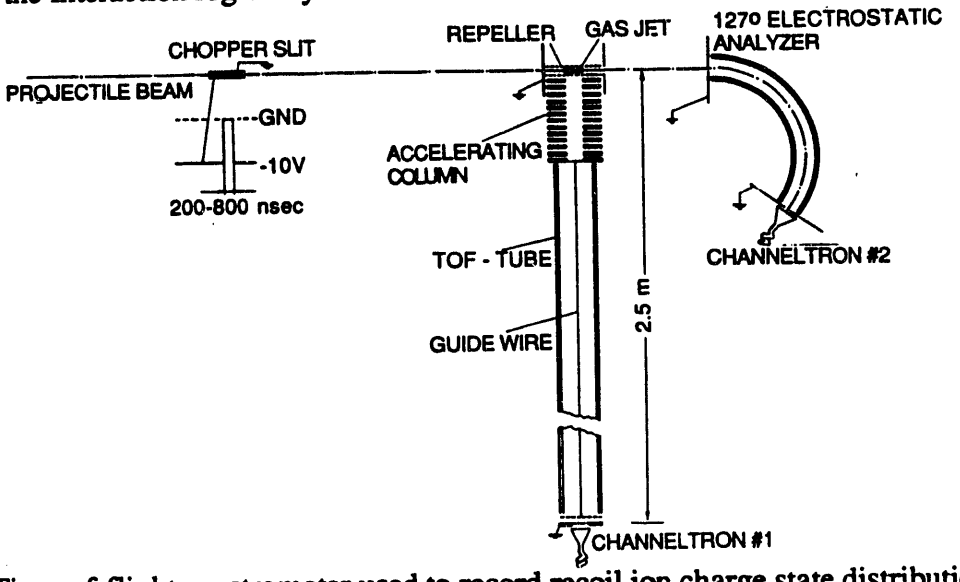

Figure 11. Time-of-flight spectrometer used to record recoil ion charge state distributions.

To prevent loss of ions in the 2.5 m long TOF drift region, a central guide wire, biased negatively at a few volts with respect to the drift tube, was used to guide the ions through the spectrometer. [13] The spectrometer was electrically isolated from ground and could be floated at a high voltage. An accel/decel lens in front of the interaction region (not shown) could speed up or slow down the ions entering the spectrometer. The relative recoil ion charge state fraction as a function of projectile charge q in 2.3 qkeV Ar^{q+} on Ar $(6 \le q \le 16)$ is shown in figure 12.

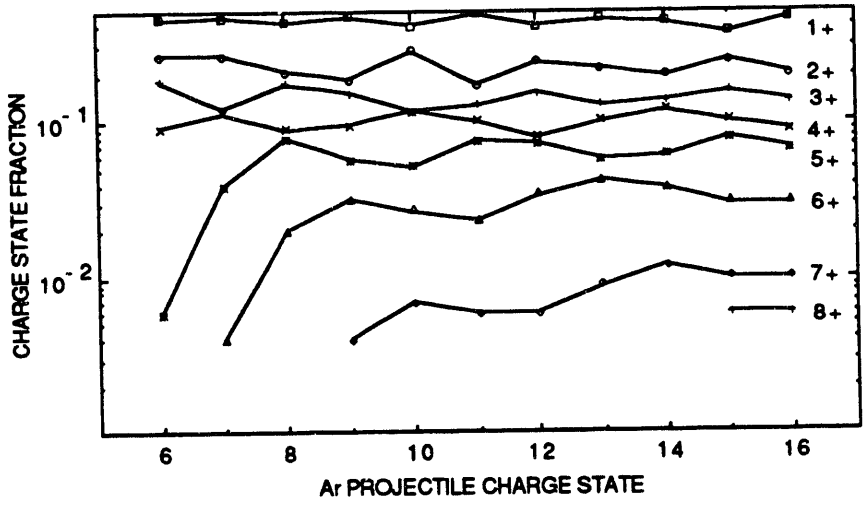

Figure 12. Fraction of recoil ions of a given charge state as a function of projectile charge q in Ar^{q+} on Ar collisions at 2.3 qkeV.

Such spectra underscore the need to take into account the relatively high recoil ion charge states in any interpretation of electron transfer processes in collisions between low energy, highly charged ions and multielectron targets.

This work was accepted for publication as a contributed paper in the proceedings of the VIth International Conference on the Physics of Highly Charged Ions held at Kansas State University, September 28-October 2, 1992. A preprint of this article can be found in the appendix.

5) Absolute total and one and two electron transfer cross sections for Ar^{8+} on Ar at 2.3 qkeV.

We measured the total charge changing cross section for Ar^{q+} on Ar ($8 \leq q \leq 16$) at 2.3 qkeV. The method and apparatus used were similar to that described in the Ar^{q+} on H_2 and He total cross section experiment (see above). The results are shown in figs. 13 a, b and c.

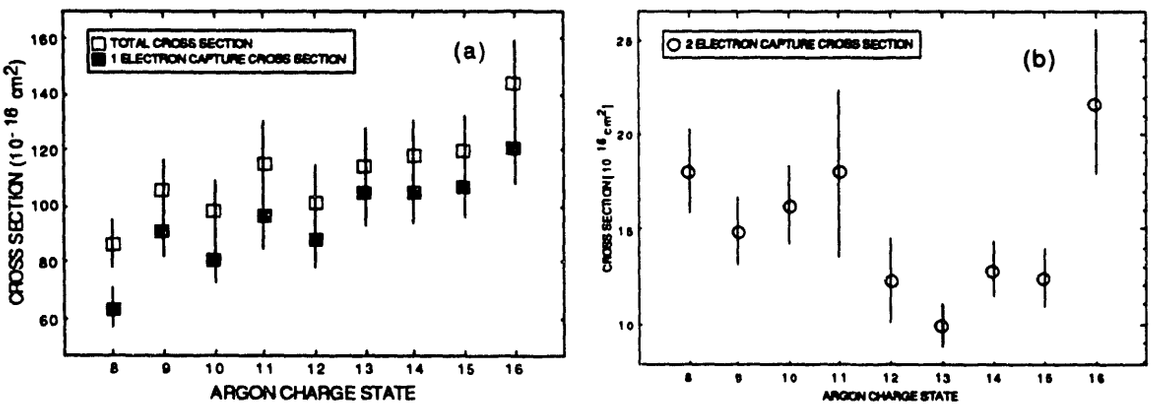

Figure 13. (a) Total and one electron transfer cross section for Ar^{q+} on Ar at 2.3 qkeV as function of q. (b) Two electron transfer cross section for Ar^{q+} on Ar at 2.3 qkeV.

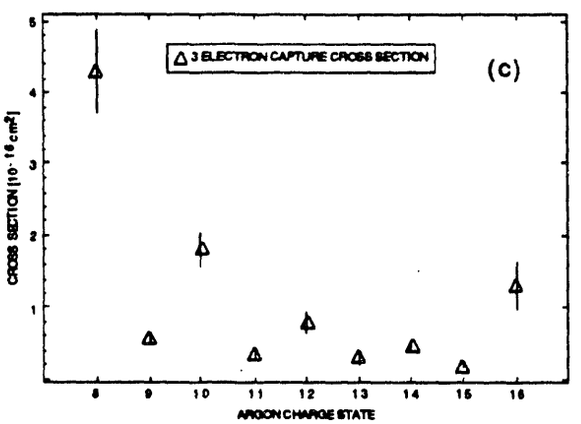

Figure 13. (c) Three electron transfer cross section for Ar^{q+} on Ar at 2.3 qkeV

The observed three electron transfer to the projectile is very small, and may even be due to

sequential single electron capture. The pressure in the gas cell is quite critical as shown in figures 14 (a) and (b). These show the charge state content of an Ar^{16+} beam after it passed through a 13 cm long gas cell at two different pressures, 7.5 x 10^{-4} and 3.2 x 10^{-5} Torr respectively. At the higher pressure, charge states down to 11+ are present in significant amounts, whereas at 3.2 x 10^{-5} Torr on sees beams that have undergone one and two electron transfer with a very small amount of three electron transfer.

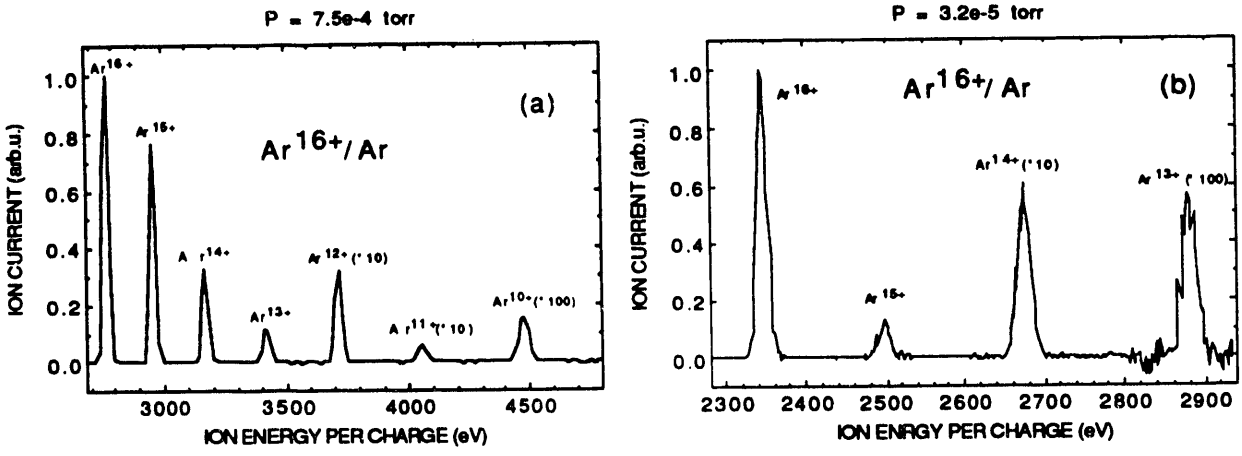

Figure 14. (a) Charge state content of an Ar^{16+} beam after passing through a 13 cm long gas cell at a pressure of 7.5 x 10^{-4} Torr. Note all the charge states present due to sequential one electron transfer. (b) Same beam after passing through the gas cell at 3.2 x 10^{-5} Torr. Mostly one and two electron transfer has occurred.

A paper based on this work is in preparation.

<u>6) Absolute total and one and two electron transfer cross sections for Ar^{8+} on Ar as a function of collision energy</u>

There have been very few absolute total and one and two electron transfer cross section measurements for highly charged ions colliding with multielectron atoms reported in the literature. As far as charges greater than or equal to eight are concerned, such measurements appear to be almost non existent. We measured the absolute total one and two electron transfer cross sections for Ar^{8+} on Ar as a function of projectile laboratory energy from 0.09 to 0.550 kev/amu. The measured cross sections include all processes which result in an argon projectile final charge state that is one or two units lower than the incident charge state.

In this experiment, a magnetically selected Ar^{8+} was decelerated to lower energies by an ion optical lens system before entering a gas cell which was electrically isolated from ground, figure 15. The gas cell is similar in design to that described in the Ar^{q+} on H_2 and He experiment in that

the absolute gas pressure in the cell was measured directly by the orifice flow method. [7,8] The cross sections were determined by the growth rate method [6] and the charges present in the beam after it passed through the cell were analyzed by a $\pi\sqrt{2}$ cylindrical electrostatic analyzer. The measured cross sections are shown in figure 16.

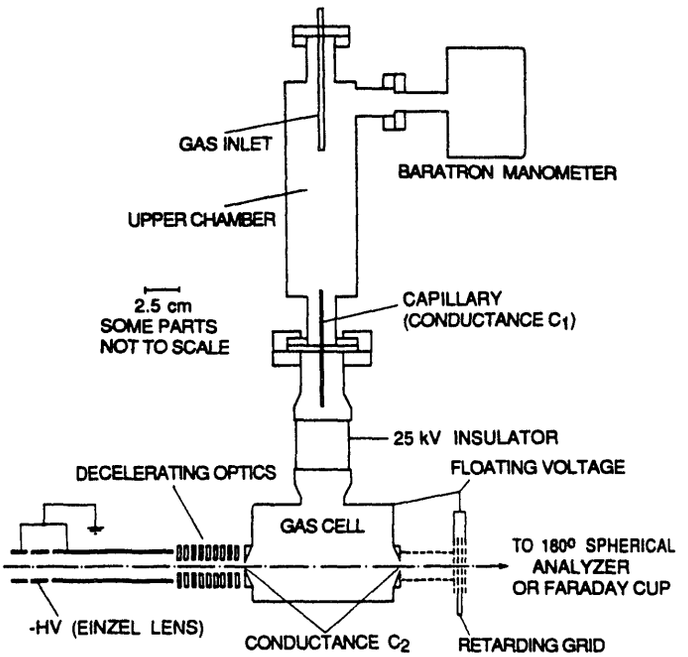

Figure 15. Experimental apparatus used to measure total and one and two electron transfer cross sections for Ar^{8+} on Ar as function of collision energy

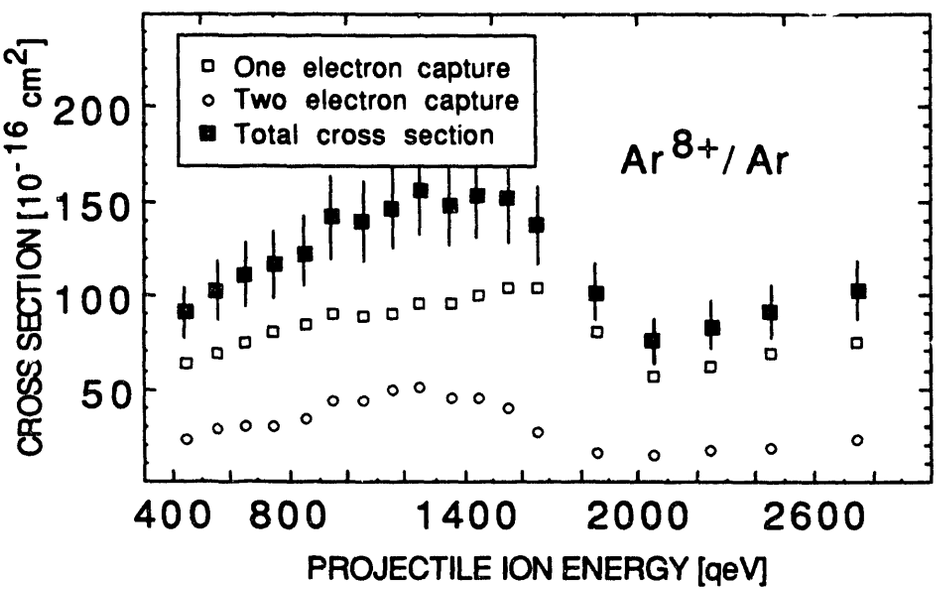

Figure 16. Measured absolute total, one and two electron transfer cross section for Ar^{q+} on Ar as function of projectile energy.

This work was accepted for publication as a contributed paper in the proceedings of the VIth International Conference on the Physics of Highly Charged Ions held at Kansas State University, September 28-October 2, 1992. A preprint of this article can be found in the appendix.

A paper based on this work is in preparation.

7) Energy gain spectroscopic study of Ar^{q+}-Ar collisions at 40 qeV

Thus far, there have been very few measurements of energy gain spectra in low energy, highly charged ion-atom collision reported in the literature. Ohtani et al. [13] have measured the energy gain spectra of bare C and O projectiles that have captured one electron from He, Nielson et al. [14] have measured energy gain spectra of Ar^{q+} $(6\leq q\leq 10)$ on Ne, Ar and Xe, and Giese et al. [15] Ar^{q+} $(4\leq q\leq 8)$ on Ar.

Magnetically selected charge states, extracted at 2.3 kV, were decelerated to 40 qeV by a combination einzel lens and decelerating lens system. The slow beam was monochromatized by a a pair of 180^{o} spherical electrostatic analyzers (mean radius 89 mm) connected in series. After passing through a gas cell (pressure ~6.0×10^{-5} Torr), the direct beam was analyzed by a similar pair of analyzers. The experimental arrangement used is shown in figure 17, and some of the 0^{o} energy gain spectra obtained are shown in figure 18.

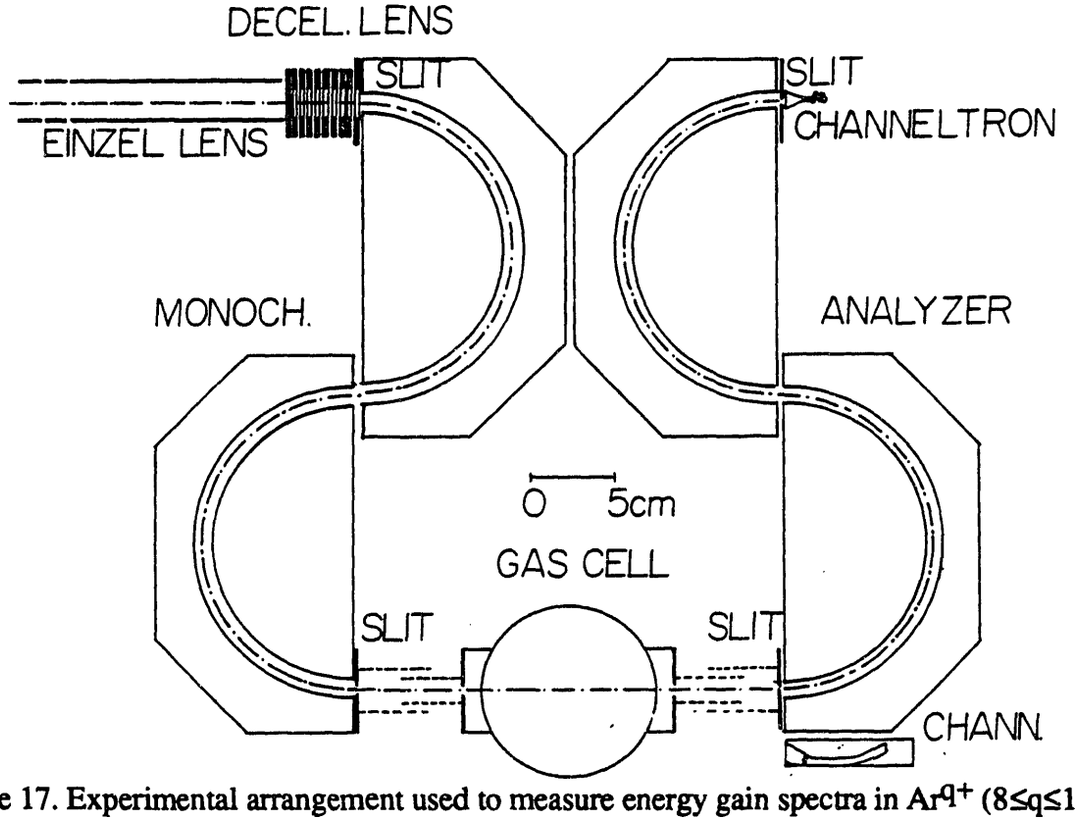

Figure 17. Experimental arrangement used to measure energy gain spectra in Ar^{q+} $(8\leq q\leq 15)$ on Ar at 40 qeV

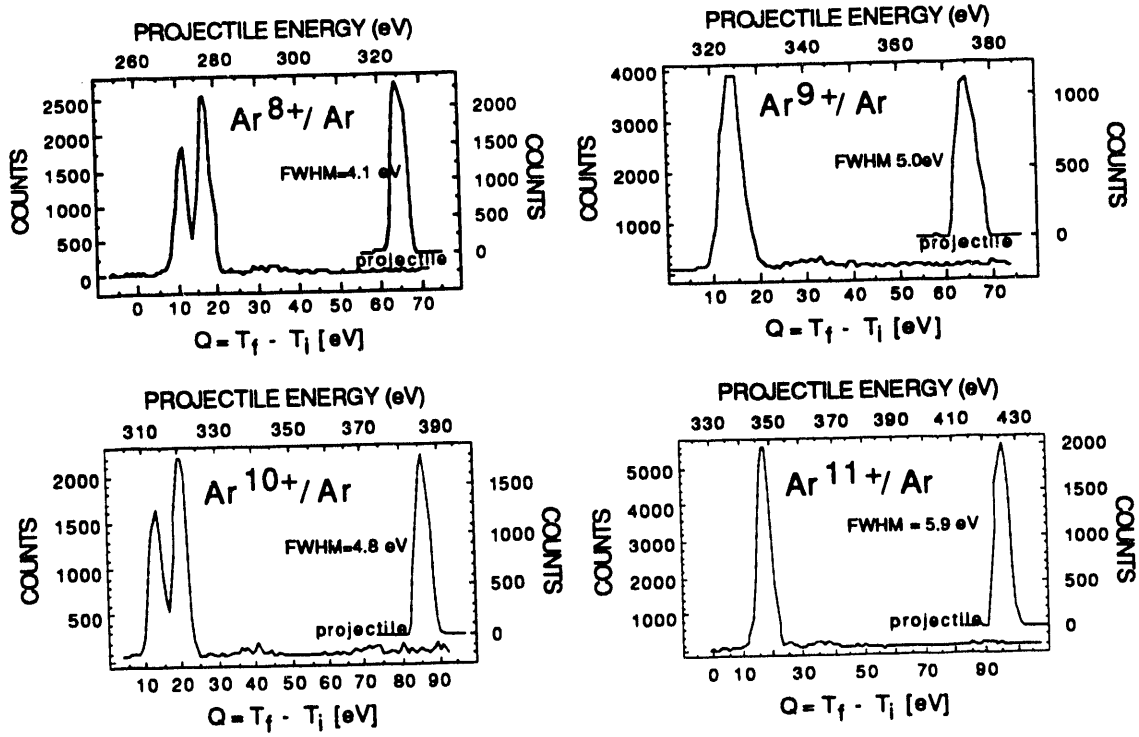

Figure 18. Some of the 0^o energy spectra obtained. The Q values are given in terms of the initial and final kinetic energies of the reactants and products *in the center of mass system.*

The spectra exhibit an even-odd projectile charge state effect in which even numbered charge states show two distinct peaks while the odd numbered charge states show only one. The reasons for this are not known at this time.

This work was accepted for publication as a contributed paper in the proceedings of the VIth International Conference on the Physics of Highly Charged Ions held at Kansas State University, September 28-October 2, 1992. A reprint of this work can be found in the appendix.

8) Energy gain spectroscopic study of Ar^{q+}-Ar collisions at low collision energies -continued

Using recently constructed electrostatic analyzer power supplies, we have re-measured the Ar^{q+} on Ar $(8 \le q \le 15)$ energy gain spectra at 0^o. The power supplies consist of two supplies, for each of which, +V/2 and -V/2 can be varied simultaneously from 0 to 500 V with 2 parts per 10^4 precision. The supplies can be controlled either manually or programed by computer. The supplies can be floated at high voltage and they replace the floating battery and potentiometer supplies used in earlier experiments. The results of the measurement for Ar^{8+} on Ar are shown in figure 19, which shows both the profile of the incident beam and the 0^o energy gain spectrum of the projectile following one electron transfer. At 30 qeV, the energy resolution was 0.27 qeV. With the new power supplies we can measure accurately the energy gain of the projectile, and

hence obtain the Q values of the reaction.

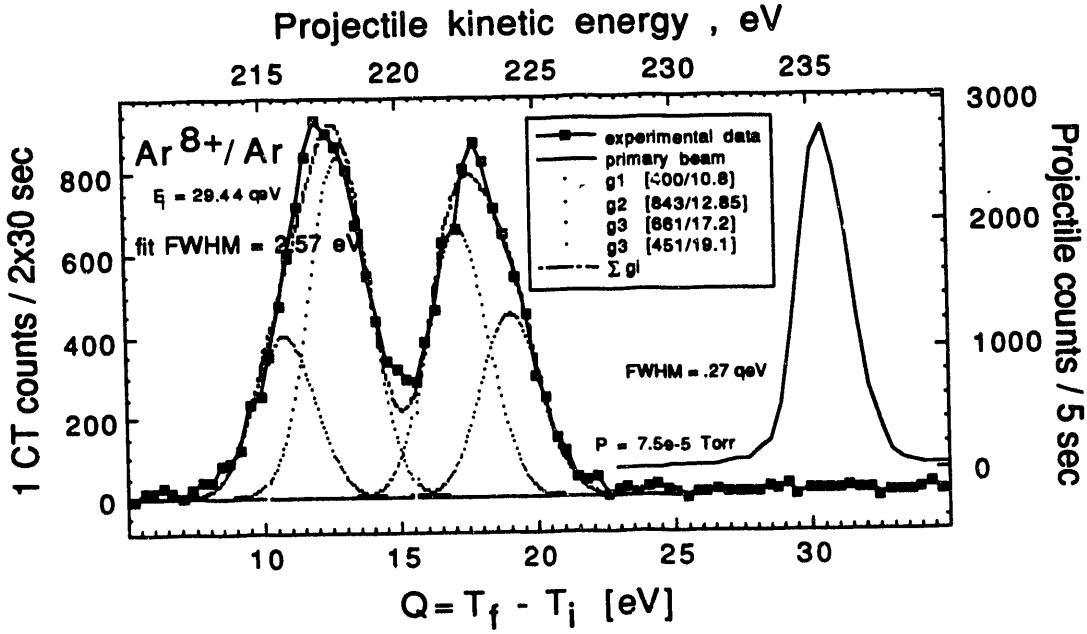

Figure 19. 0^{o} energy gain spectrum of the projectile following one electron transfer in Ar^{8+} on Ar collisions at 29.4 qeV. The Q values are given in terms of the initial and final kinetic energies of the reactants and products *in the center of mass*.

The FWHM of the incident Ar^{8+} beam was 2.16 eV. We estimate that the energy analyzer accepted particles scattered up to 2^{o}. This would contribute ~1.4 eV to the width of the energy gain peaks to give an overall FWHM of 2.57 eV. Because the energy gain (Q values) peaks are noticeably wider than the primary beam (fitted nicely by a Gaussian) we fitted the observed peaks by a number of Gaussians of constant FWHM = 2.57 eV. The best fit was obtained with four Gaussians centered at 10.8, 12.8, 17.2 and 19.1 eV respectively.

We have almost finished the analysis of this data, and an article based on this work is in preparation.

9) Ionization and dissociation of CO and N_2 in collisions with low energy, highly charged argon ions

In a continuing attempt to better understand the mechanism of multielectron transfer from many electron targets, we investigated collisions of highly charge Ar ions with multielectron atomic and molecular targets (Ne, Ar, CO and N_2). (The Ar experiments and the experimental arrangement used are described above.) The TOF spectra of the recoil ions produced in Ar^{8+} and Ar^{16+} on Ar are shown in figures 20 a and b, while 20 shows Ar^{8+} on Ne, all at 2.3 qkeV. Figure 21 shows a typical TOF spectrum of molecular ions and dissociation fragments in Ar^{11+} on CO collisions.

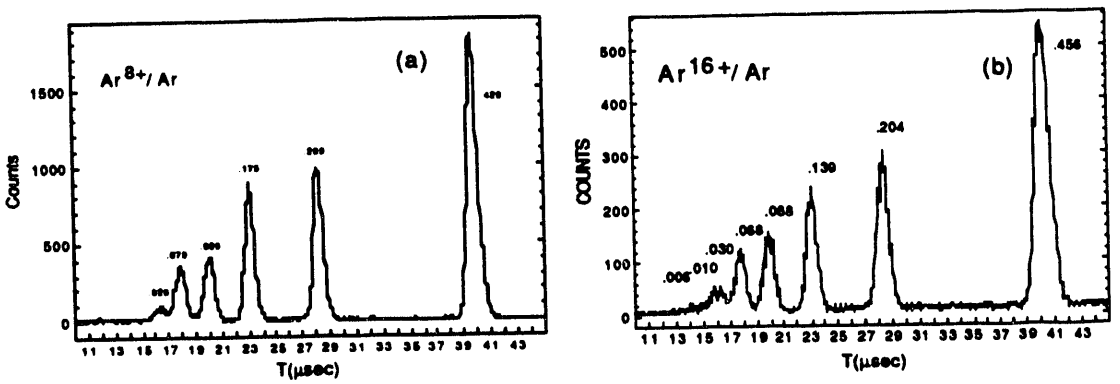

Figure 20.(a) Recoil ion charge state distribution for Ar^{8+} on Ar measured by TOF. The numbers shown indicate the fraction of a particular charge state present. The lowest charge state, 1+, occurs at the longest time of flight. (b) Ar $^{16+}$ on Ar recorded under similar conditions as (a). In this case, charge state 7+ is clearly visible.

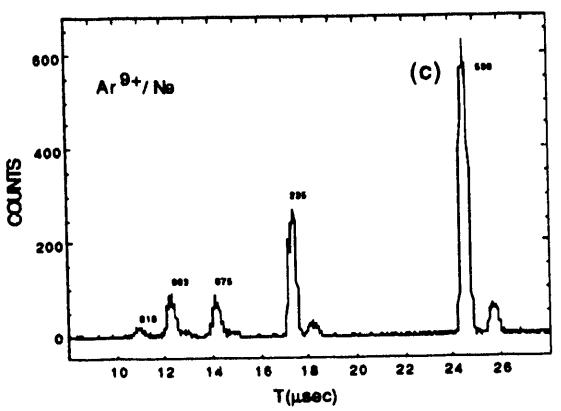

Figure 20.(c) Ne recoil ion charge state distribution in Ar^{q+} on Ne collisions. Note the heavier isotope ^{22}Ne that appears to the right of the more common ^{20}Ne peaks. The ion charge state 5+ is clearly visible.

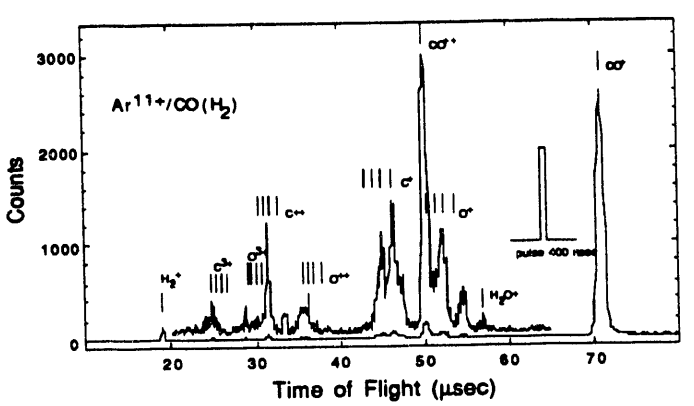

Figure 21. TOF spectrum of molecular ions and dissociation fragments in Ar^{11+} on CO collisions. (Small amounts of H_2 were introduced to help calibrate the time of flight spectrometer).

Similar spectra were observed for different Ar projectile charge states and N_2 as target. All the molecular target spectra exhibit more or less the same features regardless of the incident argon projectile charge state.

The spectra are dominated by the singly charged ions, in this case CO^+. This is in sharp contrast to highly charged ion-atom collisions in which the singly charged ion accounts for only half of the observed target charge states. The stable/long lived metastable CO^{++} molecular ion is the next most prominent feature observed. The rest of the peaks are associated with dissociation of the CO^{q+} molecule, with kinetic energies of the fragments equal to the Coulomb potential energy for different channels (e.g. $C^{3+} + O^{2+}$) evaluated at the CO molecule equilibrium separation.

The molecular target portion of this work was presented at the IX^{th} European Conference on the Dynamics of Molecular Collisions held at Prague, Czechoslovakia, August 30-September 4, 1992. A reprint of the abstract can be found in the appendix.

10) Many body theory of atomic transitions

In this work, the transition theory of Goldberger and Watson [17] was applied in a systematic manner to derive transition rates and cross sections for atomic radiative and /or non radiative processes. All rates were derived from proper solutions of the time-dependent Schrodinger equation with emphasis on situations in which the initial and final state wave functions are non orthogonal functions that belong to different self-consistent fields. The approach is particularly useful in the treatment of ionizing transitions where the outgoing free electron sees a different atomic potential from that of the initial bound electron. The transition amplitudes are expressed as perturbation expansions in which singularities due to states degenerate with the initial and final states have been removed. These perturbation expansions show clearly how the non orthogonality of the participating states leads to terms that represent "shake" processes which compare to higher-order electron correlation processes. Transition amplitudes, including all second-order processes, are derived for the following transitions: X ray, Auger, photoionization, radiative recombination, dielectronic recombination and the radiative-Auger. The expressions are compared with those frequently used by other workers.

A computer code TRANSIT was written which is based on this work. The code calculates non-relativistic wave functions from either self-consistent (Hartree-Fock-Slater), Thomas-Fermi, or hydrogenic fields. Transition rates are computed using angular and radial matrix elements calculated form these wave functions. At present, TRANSIT can calculate energies, wave functions, and radiative and non-radiative rates for atoms and ions. The code is highly modular and can easily be modified to calculate higher order processes. Figure 22 shows the total calculated K-shell fluorescence and Auger yields for the range $(5 \leq Z \leq 36)$ using a Hartree-Fock-Slater model [18] to calculate the wave functions. These calculations show the effects of initial/final

state overlap on K-shell X ray and Auger transition rates The Auger results are in excellent agreement with earlier calculations. [19]

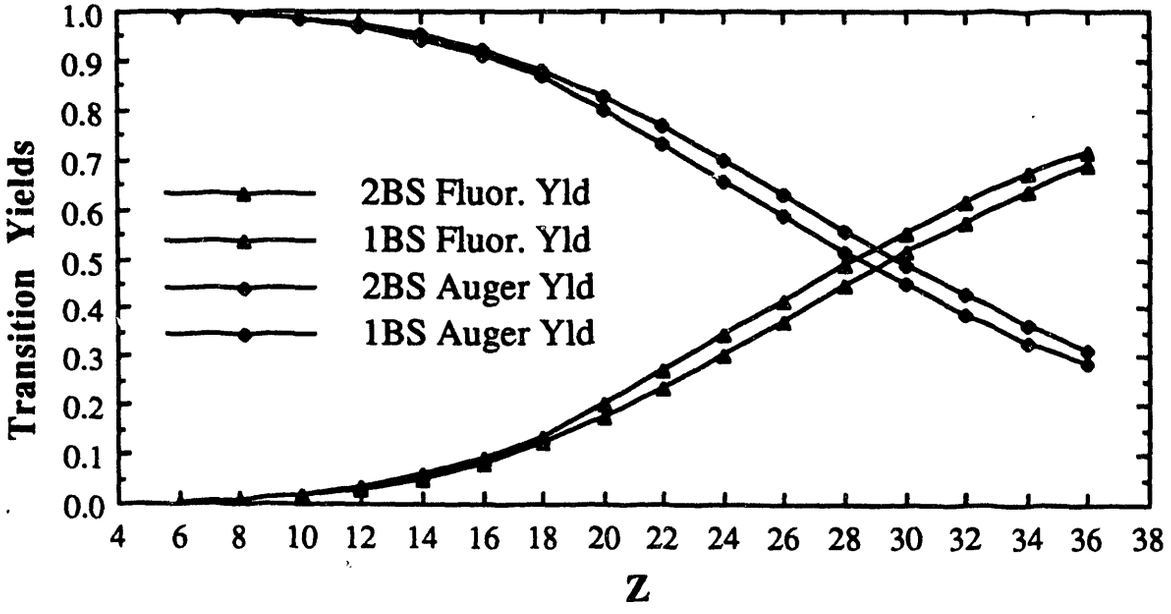

Figure 22. K-shell fluorescence and Auger yields as a function of atomic number Z. The yields were calculated using different basis sets for the initial and final state wave functions (labelled 2BS). and a single basis set for the initial and final states (labelled 1BS).

This work formed the Ph.D. thesis of C.P. Holmes and three articles based on this thesis are in preparation.

11) Ab-Initio molecular orbital calculations for the Ar^{8+}-Ar system

Adiabatic electronic energies and Born-Oppenheimer potential curves are very useful for interpreting low energy, highly charged ion-atom (molecule) collisions. For example, in order to shed light on transfer ionization processes in Ar^{q+}-Ar collisions, it is desirable to have some idea as to how the electronic states of the colliding system evolve as a function of internuclear separation. To help us interpret our electron emission data in Ar^{q+}-Ar collisions, we have calculated an electron correlation diagram for the Ar^{8+}-Ar system. The stationary states were calculated for different internuclear separations by the independent particle, Hartree-Fock molecular orbital approach within the LCAO framework. The POLYATOM series of programs [20] was used to carry out the calculation with an uncontracted [11s,8p] Gaussian basis set.

Gaussian basis sets for highly charged ions such as Ar^{8+}, which are not even discussed by quantum chemists, were obtained as follows. The exponents for the primitive Gaussians were found by non linear least squares fit (Levenberg-Marquardt method [21]) to the single particle wave

functions calculated by the Froese-Fischer MCHF code. [22] The Gaussian basis sets were built up by sequential fits to the various atomic wave functions while previously determined exponents were kept fixed. For example, in the argon case, the first few s orbital exponents could be found by fitting the 3s atomic orbital. The next few s orbitals could then be found by fitting the 2s atomic orbital while keeping the first s orbital exponents, but not their coefficients, fixed. Figure 23 shows a portion of the molecular energy levels as a function of internuclear separation calculated with POLYATOM.

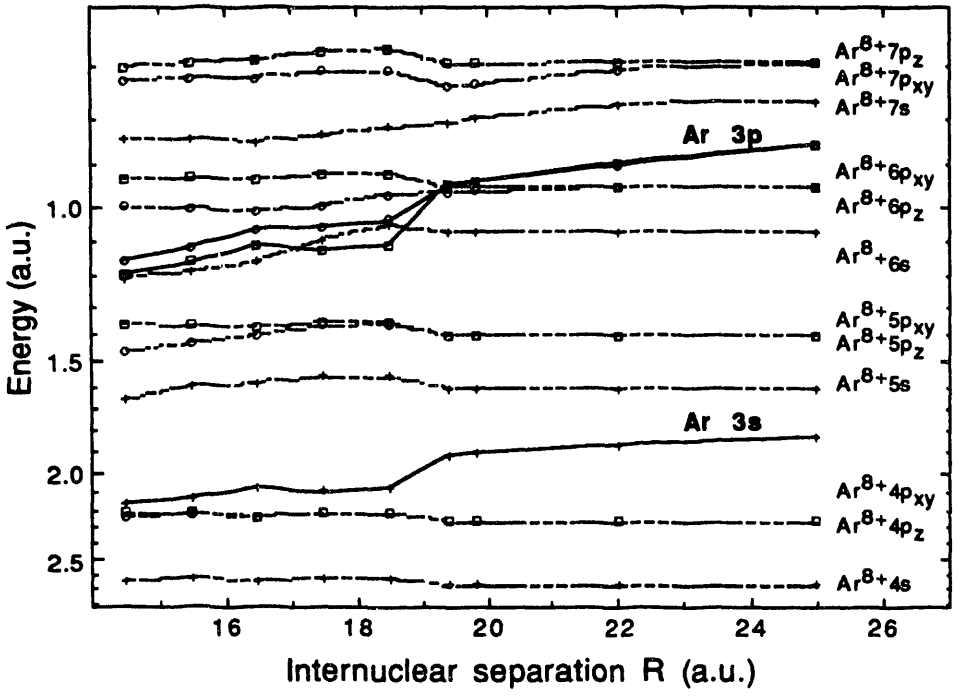

Figure 23. Electronic energies as a function of internuclear separation R for the $(ArAr)^{8+}$system . The occupied 3p and 3s orbitals of neutral argon (solid lines) cross the unoccupied Ar^{8+} 4s,p to 7s,p etc states (dashed lines) as the ion approaches the atom. At infinite internuclear separation, the Ar 3p lies above the Ar^{8+} 7s,p, and the 3s lies above the Ar^{8+} 5s (using energies calculated by POLYATOM).

Work in progress

We are analyzing and trying to understand the Ar^{q+} on Ar collision data. The correct interpretation of such collisions has to explain several observations. One, the charge state distribution of the target ions, which ranges from one to six, possibly eight for the higher charge state projectiles, two, the fact that the projectile charge state changes mostly by one unit while charge changing collisions that involve two units of charge are a factor of 10 smaller, and those involving three are 100 times smaller, and finally, the spectrum of electrons emitted in such

collisions.

The large electron transfer cross sections, around 100×10^{-16} cm^2 imply that the characteristic distance at which the reaction takes place is around 5-6 Å, or about 10 a.u.. At this distance, the potential wells of the ion and atom are sufficiently far apart so that interatomic Auger transitions involving the inner shells are unlikely, and therefore cannot contribute significantly to multiple ionization of the target.

With the help of figure 23, we can say something about the states of the projectile into which electrons may be captured. The pertinent electrons in the neutral argon target are in the 3s and 3p state. This state remains pretty much unaffected by the incident projectile until the charged ion approaches the atom within a certain distance. At this point, the 3s state goes over into the $4p\sigma$ molecular state which correlates with the 4p state of the united atom, and the 3p splits into $4d\pi$ and $5f\sigma$ states which go over into the 4d and 5f states of the united ion-atom (not shown). However, since at the low energies at which these collisions occur, we do not approach the united system case by any means, it may be more useful to look at the multiparticle energy states in the projectile that are roughly of the same energy as the 3s and 3p states in the target at ~10 a.u. internuclear separation. This means that the states of interest will be the 4s,p, 5s,p, 6s,p 7s,p of the Ar^{8+} ion with different electron populations, and the 3s and 3p states of the argon atom. (We restrict ourselves to s and p states on the ion otherwise things get complicated very quickly.)

From figure 23 we see that transfer of electrons to several excited states of the collision system is possible, and these excited states can, in turn, de-excite by emitting Auger electrons. During the collision, the 3s and 3p electrons of argon form a quasimolecular state and some of these electrons can be stranded on the projectile after the collision. Figure 24 shows a plot of the $3p_z$ molecular wave function when Ar^{8+} and Ar are separated by 20 a.u..

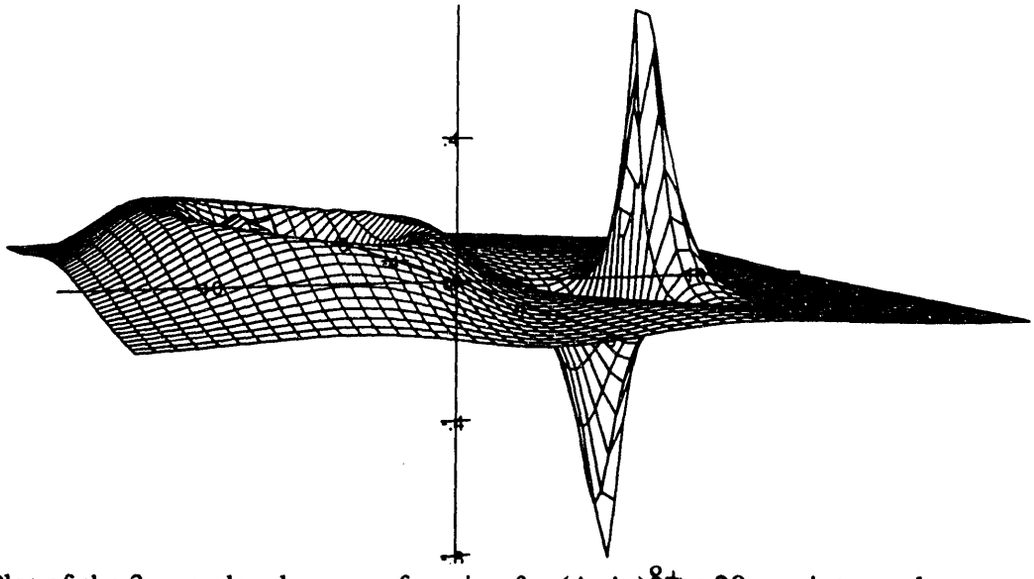

Figure 24. Plot of the $3p_z$ molecular wave function for $(ArAr)^{8+}$ at 20 a.u. internuclear separation calculated with POLYATOM. Ar is at +10, Ar^{8+} at -10.

One can see that even at this relatively large separation there is an appreciable electron density on the Ar^{8+} (centered at -10 a.u.) so it is quite possible for several electrons to end up being stranded on the Ar^{8+} as the collision partners separate. The de-excitation of the excited states of the projectile gets rid of all but one (in most cases), and sometimes two and even three electrons, so that one is left with a multiply ionized target ion and a projectile whose charge state has changed by one, two or even three units of charge. Figure 25a shows some of the pertinent energies involved in one and two electron transfer, and 25 b in three electron transfer for the ion-atom system at infinite separation. All energies were calculated using Froese-Fischer's MCHF code. [22]

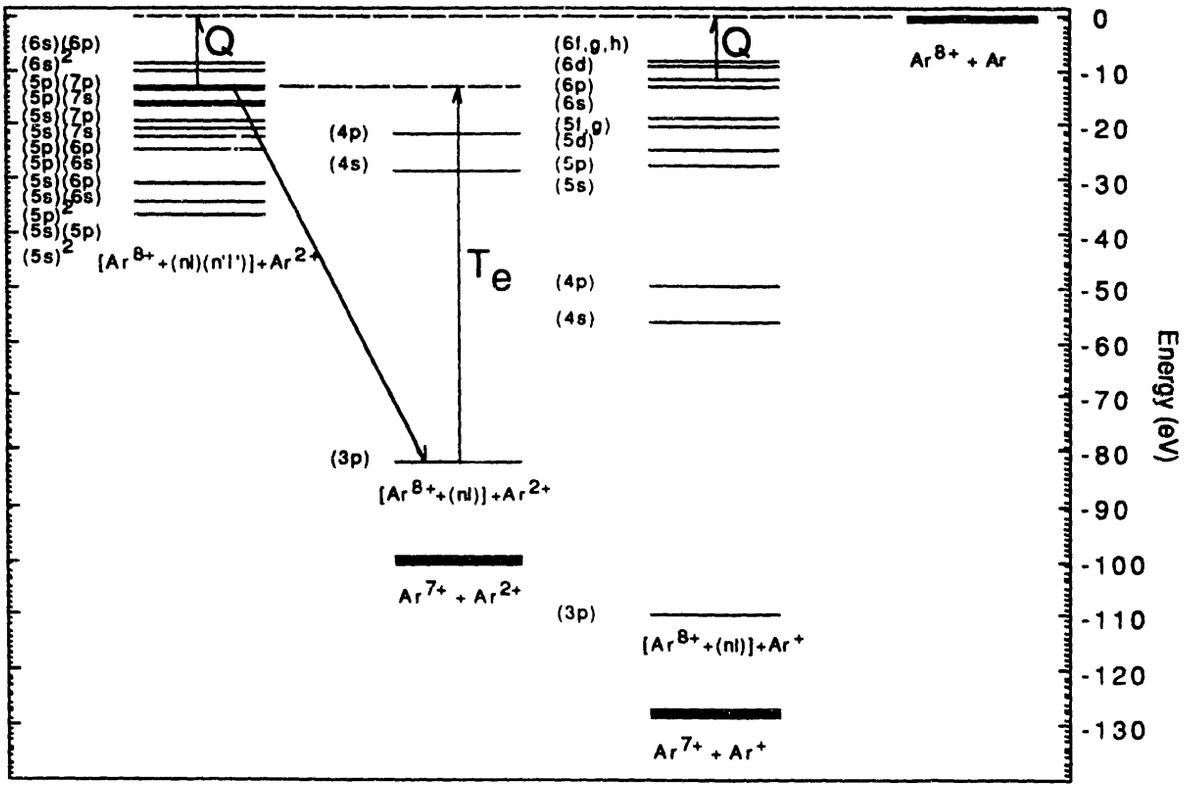

Figure 25 a. Energy level diagrams for the $[Ar^{8+}+(nl)(n'l')]$ and $[Ar^{8+}+(nl)]$ systems. The ground states are shown as thick lines. The vertical lines Q represent the energy transferred to the nuclear translational coordinates, and the line T_e represents the kinetic energy of an emitted Auger electron.

The energies plotted are the average energies of a given configuration. In the figures, the vertical lines labeled Q represent the energy taken up by the nuclear translational motion when one electron is captured into (6p), two electrons into (5p)(7p) and three electrons into $(5s)^2(7s)$ respectively. All have roughly the same Q ~10 eV. The excited state formed in single electron capture can only decay radiatively, while the (5p)(7p) state formed in two electron capture and the $(5s)^2(7s)$ state in three electron capture can decay by nonradiative transitions. In figure 25 a, the (5p)(7p)→(3p)(εl)

transition is shown. The vertical line labeled T_e represents the kinetic energy ε of the ejected Auger electron. In figure 25 b the $(5s)^2(7s)$ goes to $(5s)(4p)(\varepsilon_1 l_1)$ where T_{e1} is the kinetic

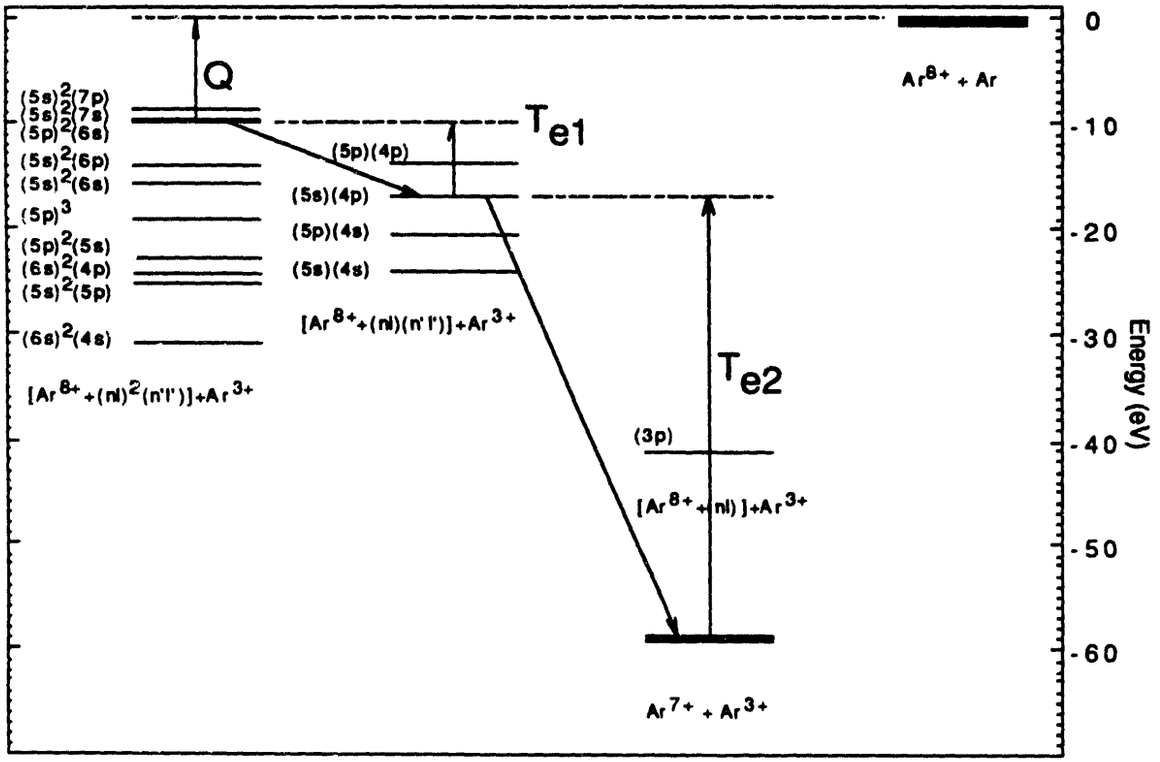

Figure 25 b. Energy level diagram for the $[Ar^{8+}+(nl)^2(n'l')]$ system. The ground states are shown as thick lines. The vertical lines Q represent the energy transferred to nuclear translation coordinates, and the lines T_e represents the kinetic energies of emitted Auger electron.

energy of the emitted electron ε_1, and the (5s)(4p) state in turn Auger decays to $(3s)(\varepsilon_2 l_2)$ where T_{e2} is the energy of the emitted electron ε_2. In this case, the $(Ar^{7+}+Ar^{3+})$ - $(Ar^{8+}+Ar)$ energy difference goes into Q (taken up by the nuclear translational motion) plus the kinetic energies T_{e1} and T_{e2} of two emitted Auger electrons. Therefore, even though three electrons were transferred, the charge state on the projectile changed by one unit only.

We also have calculated a few non radiative transition rates for selected $[Ar^{8+}+(nl)^2(n'l')]$ and $[Ar^{8+}+(nl)(n'l')]$ excited states. These are shown in Table I. Only transitions with rates greater than 10^{-4} a.u. are shown (in units of 10^{-3}). For the sake of comparison, total K shell Auger transition rates in medium Z atoms are ~30 (in units of 10^{-3} a.u.).[19]

Table I

Non-radiative transition rates (10^{-3} a.u.) for [Ar^{8+}+$(nl)^2(n'l')$] and [Ar^{8+}+(nl)(n'l')] excited states calculated with TRANSIT.

Initial state	Final state	Transition rate	Energy (eV)
$(5s)^2(7p)$	all	2.31	
	(4s)(5s)	1.80	15.3
$(5s)^2(7s)$	all	0.80	
$(5p)^2(6s)$	all	2.85	
$(5p)^2(6s)$	(4p)(5p)	1.19	3.95
	(4s)(5p)	1.30	10.8
$(5s)^2(6p)$	all	4.18	
	(4s)(5s)	3.00	9.82
$(5s)^2(6s)$	all	1.29	
	(4s)(5s)	1.00	8.22
$(5p)^3$	all	2.49	
	(4s)(5p)	1.10	1.69
$(5p)^2(5s)$	all	3.44	
	(4s)(5s)	1.58	1.31
$(6s)^2(4p)$	all	1.39	
$(5s)^2(5p)$	all	1.12	
$(6s)^2$	(4s,p)	1.06	17.3, 10.8
	(3s,p)	0.17	88.2, 71.0
(6s)(6p)	(4s,p)	1.03	19.3, 12.8
	(3s)	0.13	90.34
$(6s)^2$	(4s)	0.15	18.2
(5p)(7p)	(4s,p)	3.78	15.5, 9.01
	(3s)	0.06	86.5
(5p)(7s)	(4s,p)	1.55	14.6, 8.08
	(3s)	0.14	85.4
(5p)(6p)	(4p)	5.42	2.48
	(4s)	1.33	8.95
	(3s,p)	0.80	80.0, 62.6
(5p)(6s)	(4p)	1.38	9.22
	(4s)	1.48	7.40
	(3s)	0.26	78.4
(5s)(7p)	(4s)	2.07	12.4
	(3s)	0.20	83.5
(5s)(6p)	(4s)	3.37	5.90
	(3s)	0.34	77.0
(5s)(6s)	(4s)	1.07	4.22
	(3s)	0.11	75.1

Because most of the rates are of the order of 10^{-3} a.u. and the collision time is ~ 50 a.u., (v ~0.2 a.u., R ~10 a.u.) , Γt ~0.05, the number of decays during the collision, which is proportional to $(1-e^{-\Gamma t})$, is small. Whether or not the Auger electrons are emitted during the formation of the quasi molecule, or are stranded on the projectile and then emitted, can perhaps be determined from a detailed analysis of the electron spectra.

The above picture is consistent with the observation of so called "hollow" atoms. [23] In this case, the capture of many electrons by a slow bare or one-electron nucleus near a metallic surface leads to the formation of multiexcited bound states with many electrons in the outermost shells. The observed K x-ray hypersatellite spectra indicate Lyman-α transitions due to a different number of L and M electrons present. While x-ray spectra due to "hollow" atoms formed in isolated ion-atom collisions have not been observed to date (as far as we know) because of the tenuous density of gas targets, there is no reason why such systems should not be formed in isolated collisions.

Personnel associated with the project

The work described in this progress report was carried out mostly by Jan Vancura, postdoctoral associate, and myself, Charles P. Holmes, Jaroslav Flidr and Scott Lassell, graduate research assistants, Peter Mucha, undergraduate research assistant and James Perotti, research technician.

Publications and talks

Publications

1. "An Electron Beam Ion Source for Laboratory Experiments", Rev. Sci. Instrum., 63, 3399 (1992). (E.N. Beebe and V.O. Kostroun)
2. "External Ion Injection into an Electron Beam Ion Source", Nucl. Instr. and Meth. in Phys. Research, B69, 492 (1991). (L. Assoufid and V.O. Kostroun)
3. "Absolute Total and One and Two Electron Transfer Cross Sections for $Ar^{q+}(8\leq q\leq 16)$ on He and H_2 at 2.3 qkeV", To be published in Phys. Rev A. (J. Vancura, V. Marchetti, J. Perotti and V.O. Kostroun)
4. "Electron emissions in low energy, Ar^{q+}-Ar collisions", To be published in the proceedings of the VIth International Conference on the Physics of Highly Charged Ions held at Kansas State University, September 28-October 2, 1992. (J. Vancura and V.O. Kostroun)

5. "Absolute total and one and two electron transfer cross sections for Ar^{8+} on Ar as a function of energy", To be published in the proceedings of the VIth International Conference on the Physics of Highly Charged Ions held at Kansas State University, September 28-October 2, 1992. (J. Vancura and V.O. Kostroun)
6. "Recoil ion charge state distributions in low energy Ar^{q+}-Ar collisions", To be published in the proceedings of the VIth International Conference on the Physics of Highly Charged Ions held at Kansas State University, September 28-October 2, 1992. (J. Vancura and V.O. Kostroun)
7. "Energy gain spectroscopic study of Ar^{q+}-Ar collisions at 40 qeV", To be published in the proceedings of the VIth International Conference on the Physics of Highly Charged Ions held at Kansas State University, September 28-October 2, 1992. (J. Vancura and V.O. Kostroun)

Contributed Papers

1. "Application of Non-Orthogonal States to Atomic Transition Probabilities", Bull. Am. Phys. Soc.,36, No.4, 1331 (1991). (C.P. Holmes and V.O. Kostroun).
2. " Ionization and dissociation of CO and N_2 in collisions with low energy, highly charged argon ions", Book of abstracts of the IXth European Conference on the Dynamics of Molecular Collisions held at Prague, Czechoslovakia, August 30-September 4, 1992. (J. Vancura and V.O. Kostroun)

Theses

1. "Many-Body Perturbation Theory of Atomic Transitions", Charles P. Holmes, Ph.D Thesis, Cornell University,January 1991.

Talks

1. "Low energy highly charged argon-ion collisions with a multielectron target", Physics Department, University of Connecticut, February 24, 1992.
2. "Low energy highly charged argon-argon collisions", Invited talk GF2 at the Twelfth International Conference on the Application of Accelerators in Research & Industry, November 2-5, 1992, Denton, TX.
3. "Atomic physics with an electron beam ion source", Laboratory of Plasma Physics, Cornell University, December 2, 1992.

References

1. E.D. Donets, Sov. J. Part. Nucl. 13, 387 (1982).
2. Y. Jongen and C.M. Lyneis in *The Physics and Technology of Ion Sources*, I.G. Brown, Editor (John Wiley and Sons, Toronto 1989) Chapter 10.
3. E.D. Donets and A.I. Pikin, Sov. Phys. JETP, 43, 1057 (1977).
4. J. Arianer, A. Cabrespine and C. Goldstein, Nucl. Instrum. and Methods, 193, 401 (1982) and J. Arianer, A. Cabrespine and C. Goldstein, T. Junquera, A. courtois, G. Deschamps and M. Olivier, Nucl. Instrum. and Methods, 198, 175 (1982).
5. Y. Sato and J.H. Moore, Phys. Rev. A19, 495 (1979).
6. H. Tawara and A. Russek, Rev. Mod. Phys. 45, 178 (1973).
7. K.E. Poulter, J. of Phys. E 10, 112 (1977).
8. N.A. Florescu, Trans. of the 8th National Vaac. Soc. Symposium, Vol 1, L.E. Preuss Editor, (Pergamon, Oxford, 1962) p 504.
9. E. Everhart, Phys. Rev. 132, 2083 (1963).
10. E. Salzborn, W. Groh, A. Muller and A.S. Schlachter, Physica Scripta T3, 148 (1983).
11. A. Muller, W. Groh and E. Salzborn, in *Electronic and Atomic Collisions*,edited by J. Eichler, I.V. Hertel and N. Stolterfoht, (North Holland, Amsterdam,1984), p.371.
12. W.C. Wiley and I.H. McLaren, Rev. Sci. Instrum. 26, 1150 (1955).
13. J. Abbe, S. Amiel and R.D. McFarlane, Nucl. Instr. and Methods 120, 73 (1972).
14. S. Ohtani, Y. Kaneko, M. Kimura, N. Kobayashi, T. Iwai, A. Matsumoto, K. Okuno, S. Takagi, H. Tawara and S. Tsurubuchi, J. Phys. B, 15, L533 (1982).
15. E.H. Nielson, L.H. Andersson, A. Barany, H. Cederquist, J. Heinemeier, P. Hveplund, H. Knudsen, K.B. MacAdam and J. Sorensen J. Phys. B 18, 1789 (1985).
16. J.P. Giese, C.L. Cocke, W. Waggoner, L. N. Tunnell and S. L. Varghese, Phys. Rev., 34A, 3770 (1986).
17. M.L. Goldberger and K.M. Watson, Collision Theory, (John Wiley & Sons, New York, 1964) Chapter 8.
18. C.P. Holmes, *Many-Body Theory of Atomic Transitions*, Ph.D. Thesis, Cornell University, (1991).
19. V.O. Kostroun, M. H. Chen and B. Crasemann, Phys. Rev. A3, 533 (1971).
20. Quantum Chemistry Program Exchange QCPE Program QCMP 072, Department of Chemistry, Indiana University, Bloomington, IN.
21. W.H. Press, B.P. Flannery, S.A. Teukolsky and W.T. Vetterling, *Numeriacal Recipes, The Art of Scientific Computing*, (Cambridge University Press, New York, 1986). Sectrion 14-4
22. C. Froese-Fischer, Comp. Phys. Comm. 43, 355 (1987).
23. J.P. Briand, L. de Billy, P. Charles, S. Essabaa, P. Briand, R. Geller, J.P. Desclaux, S. Bliman and C. Ristori, Phys. Rev. Lett. 65, 159 (1990)

Appendix

Preprints of papers accepted for publication in the proceedings of the VIth International Conference on the Physics of Highly Charged Ions held at Kansas State University, September 28-October 2, 1992.

1. Electron emissions in low energy Ar^{q+}-Ar collisions (J. Vancura and V.O. Kostroun)
2. Recoil ion charge state distributions in low energy Ar^{q+}-Ar collisions (J. Vancura and V.O. Kostroun)
3. Absolute total and one and two electron transfer cross sections for Ar^{8+}on Ar as a function of energy (J. Vancura and V.O. Kostroun)
4. Energy gain spectroscopic study of Ar^{q+}-Ar collisions at 40 qeV (J. Vancura and V.O. Kostroun)

Preprint of paper presented at the IXth European Conference on the Dynamics of Molecular Collisions, held at Prague, Czechoslovakia, August 30-September 4, 1992.

5. Ionization and Dissociation of CO and N_2 in Collisions with Low Energy Highly Charged Argon Ions (J. Vancura and V.O. Kostroun)

Preprint of paper accepted for publication by Phys. Rev. A

6. Absolute Total and One and Two Electron Transfer Cross Sections for $Ar^{q+}(8\leq q\leq 16)$ on He and H_2 at 2.3 qkeV (J. Vancura, V. Marchetti, J. Perotti and V.O. Kostroun)

preprint and abstract removed; conf papers cycled separately.
ds

DATE
FILMED
9/29/93

END